Reactivity of Aniline Cation to Stepwise Solvation in Hydrogen-Bonded Molecular Clusters

Jack A. Syage

Aerophysics Laboratory, The Aerospace Corporation, P. O. Box 92957, Los Angeles, California 90009
(Received: June 8, 1988; In Final Form: October 21, 1988)

Single molecules of aniline were stepwise solvated with solvent shells M_n consisting of either NH_3, N_2H_4, CH_3OH, or H_2O and studied by mass-resolved one- and two-color resonance-enhanced multiphoton ionization (REMPI) and electron impact (EI) ionization. The influence of microsolvation was investigated for the processes of unimolecular dissociation and intracluster bimolecular hydrogen transfer and proton transfer. The solvation of unimolecular dissociation revealed a striking charge-transfer mechanism for the well-known $C_6H_5NH_2^+ \rightarrow C_5H_6^+ + HNC$ dissociation, whereby solvation with N_2H_4 led to extensive formation of $HNC{\cdot}M_n^+$. Although all the solvents studied have ionization potentials above that of aniline, only N_2H_4 has a value less than that of the fragment C_5H_6. The observed properties of intracluster hydrogen and proton transfer were strongly affected by the solute–solvent interaction. Ionization of neat solvent clusters gave rise nearly exclusively to protonated cluster ion fragments, whereas the presence of aniline impeded protonation for any donor/acceptor combination. Hydrogen transfer from solvent to the aniline cation to form $C_6H_5NH_3^+{\cdot}M_n$ was greater for CH_3OH than for NH_3, the latter reaction occurring only for values of $n \geq 3$ by REMPI excitation. Cluster ion protonation was enhanced and occurred for all values of n by EI excitation. Proton transfer from aniline to M_n to form H^+M_n was strongly dependent on M_n proton affinity, which for a particular solvent generally increased with n. Consequently, a solvent size threshold for formation of H^+M_n was observed for NH_3 ($n \geq 3$), N_2H_4 ($n \geq 2$), CH_3OH (not seen, $n > 4$), and H_2O (not seen, $n > 4$). Calculated enthalpies of these reactions, by using a model that accounts for the energetics of stepwise solvation, displayed excellent correlation with the observed results.

Introduction

Over the past several years, researchers have discovered the ease with which gas-phase molecules prepared in a supersonic expansion form bonds by weak forces that are often unstable at ambient temperatures.[1-4] This behavior was at first used to gain information bearing on the nature of van der Waals interactions, structural relationships, and dissociative dynamics in dimer molecules.[3] However, it soon became apparent that clusters of almost any reasonable size could be formed under the appropriate expansion conditions,[4,5] allowing the properties of molecules to be studied in an environment that was intermediate between the gas and the condensed phase. Despite the significant information that has come from these studies, still the greatest experimental difficulty is in isolating the properties of a single cluster size. Common problems include (1) wide distributions of cluster size, (2) overlapping spectral absorptions, and (3) multiple conformers for any given cluster size. Furthermore, because of the weak forces that bind cluster molecules together, most spectroscopic probes are rather intrusive and can lead to dissociation, making it difficult to assign an observed signal to the correct parent cluster. This problem is compounded by the propensity for weakly bound clusters to undergo large geometry changes upon excitation and/or ionization. Unfavorable Franck–Condon factors can therefore frustrate even the best attempts at threshold excitation.

The present work deals with the reactivity of a single aniline cation seeded within a solvent shell M_n of varying size (typically

(1) Levy, D. H. *Adv. Chem. Phys.* **1981**, *47*, 323.
(2) Ng, C. Y. *Adv. Chem. Phys.* **1983**, *52*, 263.
(3) Janda, K. C. *Adv. Chem. Phys.* **1985**, *60*, 201.
(4) Castleman, A. W.; Kersee, R. B. *Ann. Rev. Phys. Chem.* **1986**, *37*, 525.
(5) Märk, T. D.; Castleman, A. W. *Adv. At. Mol. Phys.* **1985**, *20*, 65.

0022-3654/89/2093-0170$01.50/0

n = 1–10) consisting of either NH_3, N_2H_4, CH_3OH, or H_2O. One-color (1-C) and two-color (2-C) resonance-enhanced multiphoton ionization (REMPI) was used to excite the clusters to the ionization threshold to minimize fragmentation or to specific higher energies to initiate reactions. Mass-selective detection was used to study properties that are sensitive to stepwise solvation. The reaction pathways following variable-energy electron impact (EI) excitation were also investigated. These results complement the REMPI results because the cluster ions are formed directly and not through an excited neutral state. Not only is a different Franck–Condon region of the cluster ion potential surface accessed, but the microsolvated dissociation pathways excited by EI can be considered to occur from ionic clusters and not from neutral clusters that are then ionized by MPI.

The study of cluster reactivity forms a small subset of the cluster literature and tends to focus on hydrogen-bonded systems involving small molecules. The origin of these studies, beginning with the pioneering work of Kebarle and co-workers,[6,7] predates the use of supersonic expansions as a widespread laboratory tool. Important work is still being reported using low- and high-pressure flow tube cluster techniques.[6-9] Most groups today use molecular beam photoionization to study cluster properties, although several groups, including Castleman,[10] Stace,[11] Garvey and Bernstein,[12] Nishi and Shinohara,[13] and their respective co-workers, have also made effective use of EI excitation in a supersonic cluster source mass spectrometer to study solvated ion–molecule reactions.

The solvation of large molecules (e.g., aromatics) by molecules rather than rare-gas atoms has commanded less attention. Work in this area usually centers on the role of van der Waals (vdW) bonding interactions on cluster geometry,[14-17] electrostatic interactions on hypochromic shifts in transition frequencies[14-22] and ionization potentials,[20-22] and liquid–solid phase-transition behavior.[23,24] Studies focusing on the reactivity of a large molecule in a microsolvent shell are even less common; most tend to deal with so-called "soft" chemistry (e.g., charge transfer[16,25-28] and intermolecular vdW bond dissociation[29-31]). Notable exceptions, however, do exist.[32-35] In a very important study, Felker and Zewail measured the picosecond dynamics of hydrogen-bond dissociation for stepwise solvation of isoquinoline.[32] In another example, Cheshnovsky and Leutwyler demonstrated that α-naphthol·$(NH_3)_n$ undergoes a proton transfer only for solvation involving $n \geq 4$.[33] Finally, in a recent paper, Brutschy et al. reported on intracluster proton transfer involving methylated benzene cation clustered with polar solvent molecules.[34]

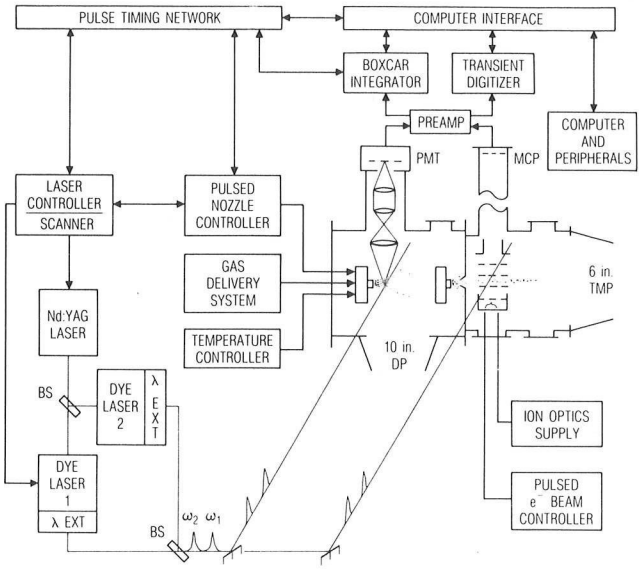

Figure 1. Schematic of the experimental apparatus. In the present work, 2-C excitation was achieved by using a single dye laser and the second, third, or fourth harmonic of the Nd:YAG laser. Symbols are defined as follows: MCP = microchannel plate detector; PMT = photomultiplier tube; TMP = turbomolecular pump; DP = diffusion pump; BS = beam splitter; λ EXT = wavelength extension components. Free jet fluorescence detection was not used in the present study.

In the present investigation, emphasis was placed on how sequential solvation promotes or quenches "hard" chemistry (e.g., fragmentation and rearrangement). Aniline was chosen for this work because its unimolecular ion fragmentation properties have been extensively studied.[36,37] The molecule also permits a study of intracluster acid–base type chemistry such as dissociative hydrogen transfer from solvent to form protonated aniline cation

(6) Kebarle, P. *Ann. Rev. Phys. Chem.* **1977**, *28*, 445.
(7) (a) Hogg, A. M.; Kebarle, P. *J. Chem. Phys.* **1965**, *43*, 449. (b) Searles, S. K.; Kebarle, P. *J. Phys. Chem.* **1968**, *72*, 742.
(8) Smith, D.; Adams, N. G.; Henchman, M. J. *J. Chem. Phys.* **1980**, *72*, 4951.
(9) (a) Viggiano, A. A.; Date, F.; Paulson, J. F. *J. Chem. Phys.* **1988**, *88*, 2469. (b) Carlon, H. R.; Harden, C. S. *Appl. Opt.* **1980**, *19*, 1776.
(10) (a) Kay, B. D.; Hofmann-Sievert, R.; Castleman, A. W. *Chem. Phys.* **1986**, *102*, 407. (b) Sievert, R.; Čadež, I.; Van Doren, J.; Castleman, A. W. *J. Phys. Chem.* **1984**, *88*, 4502.
(11) (a) Stace, A. J. *J. Am. Chem. Soc.* **1985**, *107*, 755. (b) Stace, A. J.; Moore, C. *J. Am. Chem. Soc.* **1983**, *105*, 1814. (c) Stace, A. J.; Shukla, A. K. *J. Am. Chem. Soc.* **1982**, *104*, 5314.
(12) (a) Garvey, J. F.; Bernstein, R. B. *Chem. Phys. Lett.* **1988**, *143*, 13. (b) Garvey, J. F.; Bernstein, R. B. *J. Am. Chem. Soc.* **1987**, *109*, 1921. (c) Garvey, J. F.; Bernstein, R. B. *J. Phys. Chem.* **1986**, *90*, 3577. (d) Garvey, J. F.; Bernstein, R. B. *Chem. Phys. Lett.* **1986**, *126*, 394.
(13) (a) Shinohara, H.; Nishi, N. *Chem. Phys. Lett.* **1982**, *87*, 561. (b) Shinohara, H.; Nishi, N.; Washida, N. *Chem. Phys. Lett.* **1984**, *106*, 302.
(14) Bombach, R.; Honegger, E.; Leutwyler, S. *Chem. Phys. Lett.* **1985**, *118*, 449.
(15) Carrasquillo, E. M.; Zwier, T. S.; Levy, D. H. *J. Chem. Phys.* **1985**, *83*, 4990.
(16) (a) Warren, J. A.; Bernstein, E. R.; Seeman, J. I. *J. Chem. Phys.* **1988**, *88*, 871. (b) Schauer, M.; Law, K. S.; Bernstein, E. R. *J. Chem. Phys.* **1985**, *82*, 736.
(17) Abe, H.; Mikami, N.; Ito, M. *J. Phys. Chem.* **1982**, *86*, 1768.
(18) Montoro, T.; Jouvet, C.; Lopez-Campillo, A.; Soep, B. *J. Phys. Chem.* **1983**, *87*, 3582.
(19) (a) Kobayashi, T.; Honma, K.; Kajimoto, O.; Tsuchiya, S. *J. Chem. Phys.* **1987**, *86*, 1111. (b) Kobayashi, T.; Kajimoto, O. *J. Chem. Phys.* **1987**, *86*, 1118.
(20) (a) Hagar, J.; Ivanco, M.; Smith, M. A.; Wallace, S. C. *Chem. Phys. Lett.* **1985**, *113*, 503. (b) Hagar, J.; Ivacno, M.; Smith, M. A.; Wallace, S. C. *Chem. Phys.* **1986**, *105*, 397.
(21) (a) Hagar, J.; Wallace, S. C. *J. Phys. Chem.* **1985**, *89*, 3833. (b) Hagar, J. W.; Leach, G. W.; Demmer, D. R.; Wallace, S. C. *J. Phys. Chem.* **1987**, *91*, 3750.
(22) Gonohe, N.; Abe, H.; Mikami, N.; Ito, M. *J. Phys. Chem.* **1985**, *89*, 3642.
(23) (a) Amar, F. G.; Berry, R. S. *J. Chem. Phys.* **1986**, *85*, 5943. (b) Jellinek, J.; Beck, T. L.; Berry, R. S. *J. Chem. Phys.* **1986**, *84*, 2783. (c) Beck, T. L.; Jellinek, J.; Berry, R. S. *J. Chem. Phys.* **1987**, *87*, 545.
(24) (a) Schriver, K. E.; Paguia, A. J.; Hahn, M. Y.; Honea, E. C.; Camarena, A. M.; Whetten, R. L. *J. Phys. Chem.* **1987**, *91*, 3131. (b) Stace, A. J.; Bernard, D. M.; Crooks, J. J; Reid, K. L. *Mol. Phys.* **1987**, *60*, 671.
(25) Gibson, E. M.; Jones, A. C.; Taylor, A. G.; Bouwman, W. G.; Phillips, D.; Sandell, J. *J. Phys. Chem.* **1988**, *92*, 5449.
(26) Peng, L. W.; Dantus, M.; Zewail, A. H.; Kemnitz, K.; Hicks, J. M.; Eisenthal, K. B. *J. Phys. Chem.* **1987**, *91*, 6162.
(27) Kamei, S.; Abe, H.; Mikami, N.; Ito, M. *J. Phys. Chem.* **1985**, *89*, 3636.
(28) Castella, M.; Tramer, A.; Piuzzi, F. *Chem. Phys. Lett.* **1986**, *129*, 112.
(29) (a) Boesiger, J.; Leutwyler, S. *Chem. Phys. Lett.* **1986**, *126*, 238. (b) Leutwyler, S.; Even, U.; Jortner, J. *J. Chem. Phys.* **1983**, *79*, 5769.
(30) (a) Bernstein, E. R.; Schauer, M. *J. Chem. Phys.* **1984**, *80*, 207. (b) Yamanouchi, K.; Watanabe, H.; Koda, S.; Tsuchiya, S. *Chem. Phys. Lett.* **1984**, *107*, 290.
(31) (a) Knee, J. L.; Khundkar, L. R.; Zewail, A. H. *J. Chem. Phys.* **1987**, *87*, 115. (b) Semmes, D. H.; Baskin, J. S.; Zewail, A. H. *J. Am. Chem. Soc.* **1987**, *109*, 4104.
(32) Felker, P. M.; Zewail, A. H. *Chem. Phys. Lett.* **1983**, *94*, 448, 454.
(33) (a) Cheshnovsky, O.; Leutwyler, S. *J. Chem. Phys.* **1988**, *88*, 4127. (b) Cheshnovsky, O.; Leutwyler, S. *Chem. Phys. Lett.* **1985**, *121*, 1.
(34) Brutschy, B.; Janes, C.; Eggert, J. *Ber. Bunsen-Ges. Phys. Chem.* **1988**, *92*, 74.
(35) (a) Mikami, N.; Suzuki, I.; Okabe, A. *J. Phys. Chem.* **1987**, *91*, 5242. (b) Kajimoto, O.; Yamasaki, K.; Arita, K.; Hara, K. *Chem. Phys. Lett.* **1986**, *125*, 184.
(36) (a) Kühlewind, H.; Neusser, H. J.; Schlag, E. W. *J. Chem. Phys.* **1985**, *82*, 5452. (b) Proch, D.; Rider, D. M; Zare, R. N. *Chem. Phys. Lett.* **1981**, *81*, 430.
(37) Baer, T.; Casey, T. E. *J. Chem. Phys.* **1982**, *76*, 1304.

and dissociative proton transfer from aniline cation to solvent to form protonated solvent. For this latter class of reactions, an attempt was made to model the energetics of gas-phase protonation as it evolves toward solution-phase behavior (i.e., "dissolve") by the successive addition of single solvent molecules.

Experimental Section

Molecular Beam Mass Spectrometer. The supersonic molecular beam time-of-flight (TOF) mass spectrometer has been described before[38] and is illustrated wth a few recent modifications in Figure 1. The vacuum system consists of differently pumped source and ionization chambers. A temperature-controlled magnetic solenoid pulsed nozzle in the source chamber is used for the supersonic expansion, which enters the ionization chamber through a 1-mm-diameter skimmer. Typical expansion conditions are 50 psi of He, 500-μm nozzle diameter, 2-cm nozzle–skimmer distance, and 350-μm pulse width. The ambient base pressure in the ionization chamber is typically 3×10^{-8} Torr, rising to about 2×10^{-7} Torr during operation of the pulsed nozzle at 10 Hz. The extent of clustering is very sensitive to the relative delay between the excitation source (laser or electron beam) and the pulsed valve firing. This effect has been documented in earlier studies.[33,39] By excitation at the extremities of the gas pulse, it is possible to suppress larger clusters and still form a high yield of the singly solvated dimer. This should prove important in photodissociation experiments by helping to remove interferences from dissociation of larger clusters.

The acceleration grids for the TOF mass spectrometer consist of the standard Wiley and McLaren three-grid configuration.[40] We use 1-cm grid spacings, a 1-m drift tube, and typical extraction and acceleration fields of 100–200 and 1500–2000 V/cm, respectively. Deflector plates are used near the ion source to compensate for the forward velocity of the molecular beam. Ion signals are collected by measuring current versus ion TOF using a microchannel plate detector. The active area of about 20-mm diameter does not allow uniform detection efficiency over a wide mass range; hence, the deflector voltage is adjusted to emphasize a mass region of interest. Relative intensities are therefore justified only for near-lying ion mass signals ($\Delta m/m \sim 0.3$). The widths of the TOF peaks for moderate masses (up to 200 amu) are about 20 ns. This corresponds to a unit mass resolution in excess of 500 amu. When necessary, a fast amplifier is used to increase the signal level, which broadens the peaks to 30–40 ns and in turn reduces mass resolution to about 100–200 amu. Mass spectra are recorded by using a 125-MHz bandwidth transient digitizer interfaced to an IBM AT computer.

The pulses were mildly focused by using a 30-cm focal length spherical lens positioned to bring the light to a focus about 3–5 cm before crossing the molecular beam. for the 2-C REMPI experiments, the ω_2 pulse was typically delayed (optically) by 3 ns from the ω_1 pulse. The laser pulse widths are about 4–6 ns.

Electron Impact Ion Source. A pulsed EI ion source, based on the design of Pollard and Cohen,[41] has been adapted for use in a scanning electron energy mode. A full description of the device and the variable-energy mode of operation has been described in a previous paper.[42] The electron beam is collimated to a diameter of approximately 5 mm to ensure complete overlap with the molecular beam. A gate pulse of 400 ns allows the electron beam to cross the molecular beam under field-free conditions. About 200 ns following the electron beam pulse, a 150-V pulse of 6-μs duration is applied to the repeller grid, which is biased at 1500 V dc. The duration is sufficient to extract all ions into the TOF mass spectrometer.

Sample Preparation. Solvated aniline clusters were prepared by a variety of procedures. In most cases, the aniline was deposited in a sample holder contained in the temperature-controlled pulsed nozzle. The temperature was maintained at 60 °C to give an aniline vapor pressure of about 6 Torr. In the case of ammonia solvation, a 2-L high-pressure cylinder was made up containing 10% ammonia in helium. This mixture was used as the carrier gas at a typical pressure of 50 psi (i.e., a mole ratio of about 1:50:500 for aniline/ammonia/helium). The water and methanol solvation was achieved by passing the helium flow through a bubbler containing either of these solvents. The room-temperature bubbler provided aniline/solvent/helium mole ratios of about 1:15:500 and 1:6:500 for methanol and water, respectively. The hydrazine solvation was accomplished by using reagent grade hydrazine, which contains aniline as a distillation impurity to about 0.3%. For minimization of decomposition, a Teflon-coated pulsed valve, Teflon tubing, and a fritted glass bubbler were used and operated at room temperature. For safety reasons, the helium carrier pressure was limited to 25 psi. This arrangement allowed typical mole ratios of about 1:300:30000.

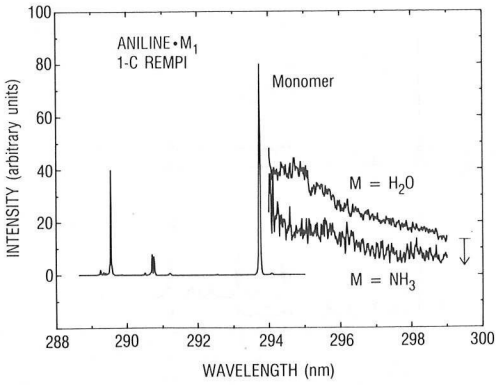

Figure 2. Mass and wavelength resolved 1-C REMPI excitation spectra for monomeric and singly solvated aniline. The A·H_2O spectrum is offset by the amount indicated. Ionization signal was normalized to the square of the laser pulse energy (nominally 0.10 mJ). Expansion conditions and mole ratios are given in the Experimental Section.

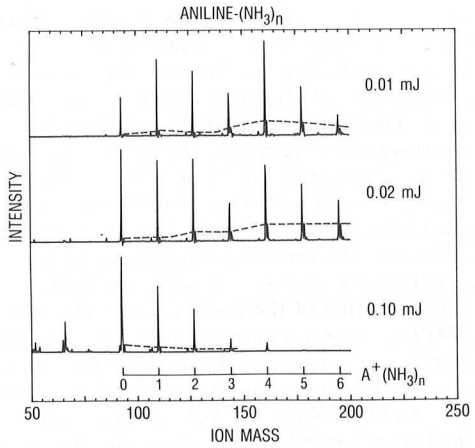

Figure 3. 1-C REMPI/MS of A–$(NH_3)_n$ clusters as a function of 295-nm pulse energy. The dotted line represents the intensity distribution of the protonated species AH^+–$(NH_3)_n$.

Results

The reactivity of aniline within a solvent shell is the subject of this work and will be discussed in depth with regard to solvated unimolecular fragmentation and intracluster proton cluster as a function of excitation source and solvent size. First we present the body of data to assist in this discussion, as well as to discuss other microsolvation effects not directly related to reactivity.

Aniline–$(NH_3)_n$. The $S_1(\tilde{A}^1B_2) \leftarrow S_0(\tilde{X}^1A_1)$ origin transition of aniline was red-shifted by about 400 cm^{-1} by a single solvent molecule (versus 293.77 nm for aniline monomer). The absorption is structureless as shown in Figure 2 (and discussed below). The overlapping spectra for the successively solvated aniline gives rise to 1 + 1 REMPI mass spectra exhibiting an extensive distribution of cluster sizes for single wavelengths of light (chosen to the red of the aniline monomer (0,0) transition). The ionization potential

(38) Syage, J. A.; Pollard, J. E.; Cohen, R. B. *Appl. Opt.* **1987**, *26*, 3516.
(39) Squire, D. W.; Bernstein, R. B. *J. Phys. Chem.* **1984**, *88*, 4944.
(40) Wiley, W. C.; McLaren, I. H. *Rev. Sci. Instrum.* **1955**, *26*, 1150.
(41) Pollard, J. E.; Cohen, R. B. *Rev. Sci. Instrum.* **1987**, *58*, 32.
(42) Syage, J. A. *Chem. Phys. Lett.* **1988**, *143*, 19.

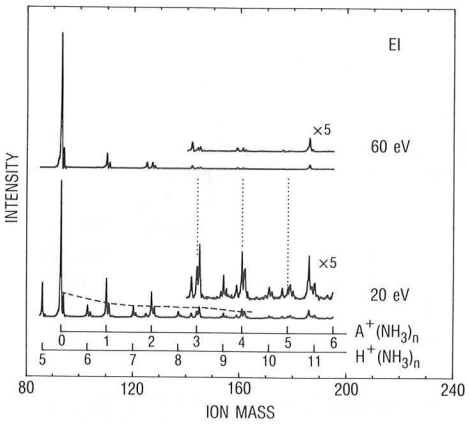

Figure 4. EI/MS of $A-(NH_3)_n$ clusters for two different e^- excitation energies. The dotted line represents the intensity distribution of the $AH^+-(NH_3)_n$ signal.

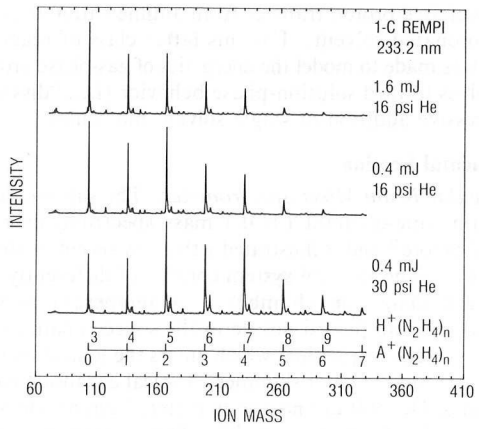

Figure 5. 1-C REMPI/MS of $A-(N_2H_4)_n$ clusters as a function of 233-nm pulse energy and backing pressure.

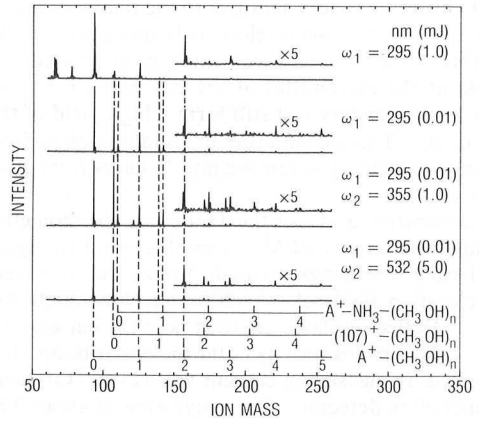

Figure 6. 1-C and 2-C REMPI/MS for the precursor clusters $A-(CH_3OH)_n$, $A-NH_3(CH_3OH)_n$, and $(107)-(CH_3OH)_n$. The ω_2 pulse was delayed 3 ns with respect to the ω_1 pulse.

I_p of aniline (7.7 eV) is considerably less than any of the solvents; hence, the positive charge resides on aniline, with charge density greatest on the aromatic ring.[43] The power dependence for 1-color (1-C) $2\omega_1$ ionization is illustrated in Figure 3. The aniline cation (henceforth A^+) is the absorbing species in the clusters and leads to solvent evaporation more readily than fragmentation. Essentially no aniline protonation occurs by NH_3 solvation for values of $n < 3$ [the weak features at $(93 + 1) + 17n$ amu are due mostly to natural-abundance ^{13}C in aniline]. Increased protonation for larger solvent sizes is discussed in depth in a later section. A stable solvation shell occurs at $n = 4$, possibly reflecting a bonding network similar to that of the stable cluster $NH_4^+(NH_3)_4$.[44]

2-C REMPI mass spectra were recorded to provide information on the properties of cluster threshold ionization and resonance ion dissociation. The ionization energy of aniline is expected to decrease by about 0.4 eV (to ~7.3 eV) upon complexation with a single hydrogen-bonded solvent molecule, on the basis of measured ionization potentials of other heteroaromatic molecules complexed to the same solvent molecules considered here.[20-22] 2-C REMPI involving a resonant 295-nm (0.05 mJ) excitation pulse and a 355-nm (1.0 mJ) ionization pulse (total photon energy of 7.69 eV) approximately doubles the ionization yield without changing the cluster ion distribution compared to excitation/ionization by 295 nm (0.1 mJ/pulse) alone. The ω_2 ionization, however, is about an order of magnitude greater for a photon at 295 nm than at 355 nm. Absorption by the cluster ions, leading to dissociation, was much less efficient at 355 nm than at 590 nm, as measured by the increase in the A^+ signal. This increase can occur only by cluster absorption and dissociation, as it has been shown in the past that the ion signal due to 1-C REMPI excitation of aniline monomer actually decreases with the addition of visible light due to $S_1 \rightarrow S_n$ transitions that do not efficiently ionize.[45] The absorption properties of the cluster ions observed here are consistent with the electronic structure of aromatic cations measured by molecular beam,[46] ion cyclotron resonance,[47] and photoelectron spectroscopy.[48]

Results for EI ionization are presented in Figure 4 for two different excitation energies. The spectra exhibit clear evidence of solvent evaporation with increasing energy. However, of greater consequence is an observed increase in protonation $AH^+-(NH_3)_n$ when ionizing by EI relative to REMPI (cf. Figures 3 and 4) and the far more extensive protonation observed for neat solvent clusters $(NH_3)_n$ compared to $A-(NH_3)_n$ excited by EI.

Aniline–$(N_2H_4)_n$. An attempt was made to resonantly excite and possibly ionize the solvent molecule N_2H_4. In either case, electronic relaxation to aniline (prior to N_2H_4 ionization) or electron transfer from aniline (subsequent to N_2H_4 ionization) was expected. Excitation wavelengths in the vicinity of 230 nm were chosen where N_2H_4 is expected to absorb.[49,50] Unfortunately, a strong absorption band exists for aniline in this region. The cluster ion distribution is represented for different pulse energies and backing pressures in Figure 5. The higher pulse energies used for these studies was necessary due to the low aniline densities contained in the samples used here (see Experimental Section). Even so, the cluster distribution does not show evidence of excessive dissociation [for instance $(A^+)/(A^+M) < 1$]. Negligible protonation of $A^+-(N_2H_4)_n$ by hydrogen transfer from solvent was evident for solvent sizes of $n < 3$. There is a weak series of neat $H^+(N_2H_4)_n$ clusters present in Figure 5, indicating the occurrence of either resonance ionization of neat $(N_2H_4)_n$ clusters or, more likely, dissociative proton transfer of $A^+(N_2H_4)_n$ clusters. The observed trend for protonation is that it is more extensive in the neat solvent ion clusters and increases with solvent size. These trends are discussed later.

Aniline–$(CH_3OH)_n$. The microsolvated aniline structure involving CH_3OH is more strongly bonded than the NH_3 solvated system. Figure 6 summarizes a variety of 1-C and 2-C excitation conditions. NH_3 was introduced into the sample to provide a direct comparison of the dissociation behavior for the two solvents. A

(43) King, G. W.; van Putten, A. A. G. *J. Mol. Spectrosc.* **1972**, *44*, 286.
(44) (a) Echt, O. H.; Dao, P. D.; Morgan, S.; Castleman, A. W. *J. Chem. Phys.* **1985**, *82*, 4076. (b) Shinohara, H.; Nishi, N.; Washida, N. *J. Chem. Phys.* **1985**, *83*, 1939.
(45) (a) Syage, J. A.; Wessel, J. E. *J. Chem. Phys.* **1986**, *85*, 6806. (b) Dietz, T. G.; Duncan, M. A.; Liverman, M. G.; Smalley, R. E. *Chem. Phys. Lett.* **1980**, *70*, 246. (c) Moll, D. J.; Parker, G. R.; Kupperman, A. *J. Chem. Phys.* **1984**, *80*, 4808. (d) Meek, J. T.; Sekreta, E.; Wilson, W.; Viswanathan, K. S.; Reilly, J. P. *J. Chem. Phys.* **1985**, *82*, 1741.
(46) Syage, J. A.; Wessel, J. E. *J. Chem. Phys.* **1987**, *87*, 3313.
(47) Dunbar, R. C. In *Molecular Ions: Spectroscopy, Structure and Chemistry*; Miller, T. A., Bondybey, V. E., Eds.; North-Holland: New York, 1983; p 231.
(48) Debies, T. P.; Rabalais, J. W. *J. Electron Spectrosc.* **1972**, *1*, 355.
(49) Work to be published.
(50) Willis, C.; Back, R. A. *Can. J. Chem.* **1973**, *51*, 3605.

TABLE I: Energy Data (electronvolts) Used in Calculations of Stepwise Solvation Enthalpies $\Delta H_{s,n}$

R	$D_{H^+}(R)^a$	$\Delta E_{i,i-1}(RH^+R_i)^b$ (1,0)	(2,1)	(3,2)	(4,3)	(5,4)	R	$I_p(R)^d$	$\Delta E_{i,i-1}(R^+R_i)$ (1,0)	(2,1)	(3,2)	(4,3)	(5,4)
aniline	9.01						aniline	7.7					
NH_3	8.77	1.08	0.76	0.60	0.54	0.35	NH_3	10.17	0.79[e] (0.45)[h]	0.55[f]	0.35[g]	0.20[g]	0.16[g]
N_2H_4	8.88						N_2H_4	8.74					
CH_3OH	7.90	1.44	0.92	0.70	0.59	0.54	CH_3OH	10.84	(0.47)[h]				
H_2O	7.36	1.37 (0.82)[c]	0.85 (0.63)[c]	0.78 (0.54)[c]	0.55	0.50	H_2O	12.6	(0.51)[h]			0.24[i]	

Bond Energies[j]

NH_2–H	4.66	$HOCH_2$–H	4.08	PhNH–H	3.82
H_2NH–H	4.34[k]	H_3C–OH	4.00	PhNH–CH_3	3.10
H_2N–NH_2	2.85	HO–H	5.16	Ph–H	4.83
CH_3O–H	4.53	$PhCH_2$–H	3.82	Ph–CH_3	4.43

[a] References 6 and 60. [b] Reference 61 (NH_3 data); ref 15c (CH_3OH); ref 62 (H_2O). [c] Data are for $CH_3NH_3^+(H_2O)_i$.[63] [d] Reference 59. [e] Reference 64. [f] Reference 75. [g] Estimated to give smooth convergence to the H-bonding energy of 0.16 eV for $NH_3{\cdot}(NH_3)_n$.[64] [h] Values for stabilization of ionization energy of 2-aminopyridine by single solvent molecules.[21] [i] Value for $H_2O{\cdot}(H_2O)_n$.[65] [j] Reference 66. [k] Reference 67.

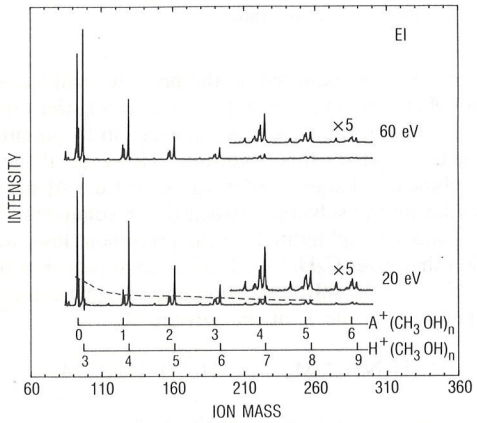

Figure 7. EI/MS of $A{-}(CH_3OH)_n$ clusters for two different e^- excitation energies. The dotted line represents the intensity distribution of the $AH^+{-}(NH_3)_n$.

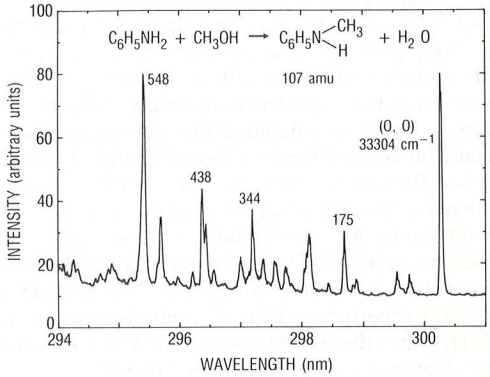

Figure 8. 1-C REMPI excitation spectrum for the reaction product (107 amu) formed from aniline and CH_3OH. The spectrum was normalized linearly to the laser pulse energy (nominally 0.10 mJ). Numbers above the vibrational features refer to displacement (in cm^{-1}) from the origin.

third set of cluster peaks is due to solvation of a reaction product (107 amu) of aniline and CH_3OH (discussed shortly). The distribution of cluster sizes for $A^+{-}(CH_3OH)_n$ is relatively unaffected by an increase in the 1-C pulse energy at 295 nm or by the addition of 5-mJ, 532-nm pulses. Similar conditions were observed to cause extensive dissociation in $A^+{-}(NH_3)_n$ clusters. Interestingly, the $A^+{-}(NH_3){-}(CH_3OH)_n$ series disappears under these dissociative conditions, indicating that in the mixed solvent system, the weakest solvent bond, namely that involving NH_3, is broken. The greater stability of the $A^+{-}(CH_3OH)_n$ clusters is also supported by EI ionization results. In Figure 7 the $A^+{-}(CH_3OH)_n$ distribution is only slightly affected by increased electron energy, in marked contrast to the results for $A^+{-}(NH_3)_n$ in Figure 4. These results suggest a stronger hydrogen-bonding network for CH_3OH compared to NH_3.

A surprising observation in the REMPI mass spectra in Figure 6 was the appearance of a mass of 107 amu that seems unique to the $A{-}(CH_3OH)_n$ system. The REMPI excitation spectrum presented in Figure 8 is well resolved, indicating that the molecule is probably a reaction product formed in the pulsed valve sample region prior to the expansion. The alternative explanation, that the product was formed in a cluster reaction, is less likely because this would be expected to impart rovibrational excitation, which in turn would be evident by the appearance of broadening and hot bands in the excitation spectrum in Figure 8. It is speculated that the product occurs by the dehydration reaction

$$C_6H_5NH_2 + CH_3OH \Rightarrow C_6H_5NHCH_3 + H_2O \qquad (1)$$

With use of bond-energy arguments (cf. Table I), reaction 1 should have an exothermicity of $\Delta H = -0.44$ eV. (Methylation of the aromatic ring is more exothermic, $\Delta H = -0.76$ eV; however, the activation energy is probably greater because it involves breaking a strong aromatic C–H bond). Gas-phase dehydration reactions involving alcohols have previously been reported.[51] In the case of methanol clusters, Morgan and Castleman[51a] observed dehydration by MPI, whereas Shulka and Stace[51b] failed to observe the same reaction by EI. Interestingly, this is the same trend observed in the present case (compare Figure 6 and 7), even though for the reasons described above, we hesitate to attribute the dehydration product to a cluster reaction. We intend to explore this issue in future work.

Aniline–$(H_2O)_n$. The reactivity of aniline cation in H_2O was limited to smaller cluster sizes. Our sample preparation, described in the Experimental Section, made use of a room-temperature bubbler; hence, the vapor pressure of H_2O (24 Torr at 25 °C) did not significantly exceed that of aniline present in the pulsed valve (~6 Torr at 60 °C). Nonetheless, there were certain properties that were clearly discernable. In accord with the other solvent systems, the nucleated clusters $A^+{-}(H_2O)_n$ did not exhibit protonation for $n < 3$ (larger clusters were too weak to judge), and threshold ionization was achieved by 2-C REMPI involving 296-nm excitation and 355-nm ionization.

Mass-Selected Excitation Spectra. 1-C and 2-C REMPI excitation spectra failed to show any resolved vibronic structure for the solvents NH_3, CH_3OH, and H_2O (N_2H_4 was not attempted in the S_1 region of aniline). Instead, broad red-shifted spectra were obtained as shown in Figure 2. This result is surprising in that highly resolved spectra have been reported for several other solvated aromatic molecules.[14-22,32-35] Congestion of the mass-selected excitation spectra caused by fragmentation of larger clusters was ruled out by demonstrating the stability of the ion

(51) (a) Shukla, A. K.; Stace, A. J. *J. Phys. Chem.* **1988**, *92*, 2579. (b) Morgan, S.; Castleman, A. W. *J. Am. Chem. Soc.* **1987**, *109*, 2867. (c) Grimsrud, E. P.; Kebarle, P *J. Am. Chem. Soc.* **1973**, *95*, 7939. (d) Bass, L. M.; Cates, R. D.; Jarrold, M. F.; Kirchner, N. J.; Bowers, M. T. *J. Am. Chem. Soc.* **1983**, *105*, 7024.

clusters to 2-C $\omega_1 + \omega_2$ threshold ionization and low-power (~0.01 mJ) 1-C two-photon ionization. Other possibilities for diffusive S_1 cluster absorptions include (i) lack of cooling during cluster growth, (ii) large geometry changes upon excitation, and (iii) charge transfer in the S_1 state due to a strong acid–base interaction. The first possibility refers to insufficient cooling of the clusters only. Judging from the highly resolved excitation spectra of aniline monomer (Figure 2) and the weak *N*-methylaniline product (Figure 8), as well as our success in recording highly resolved cluster spectra for large molecules (e.g., naphthalene),[52] there is no compelling reason to suspect the expansion conditions. The stabilization bond energy in the growing cluster can take the form of heat by vibrational relaxation (i.e., heat of condensation). For strong hydrogen-bonding complexes, this heat can be considerable and may not be cooled effectively in the downstream region of the rapidly exanding jet. The use of a hot nozzle has also been implicated in the disappearance of structured absorption by causing the clusters to be formed warm.[16a] The second possibility may be rationalized on the grounds that aniline undergoes a large $S_1 \leftarrow S_0$ change in the equilibrium geometry and force constants for the angle between the plane of the aromatic ring and the $-NH_2$ group.[43] The inversion mode in S_1 is a large amplitude motion with essentially no barrier.[53a] The solvent molecules, which are expected to hydrogen bond to the $-NH_2$ group, may be forced to undergo substantial reorientation.[53] This motion could introduce large nondiagonal Franck–Condon factors involving low-frequency intermolecular vibrations, resulting in a general broadening of the absorption bands. The third possibility above is intriguing to consider but not very likely. Aromatic amines become more acidic (less basic) in S_1[54,55] but not nearly to the extent that α-naphthol does. Yet, Cheshnovsky and Leutwyler[33] have reported that the S_1 excitation spectra of α-naphthol·$(NH_3)_n$ are vibronically resolved for $n \leq 3$; diffuse ion pair absorption features are observed only for $n > 3$.

Solvated Unimolecular Fragmentation

There is a body of literature that bears on the subject of stepwise solvation in reacting molecules,[6-13,32-35] as discussed in the Introduction. What sets the present study apart from previous work is that we consider both unimolecular and bimolecular reactions in large molecules. In particular, we have chosen to investigate the influence of solvation on known unimolecular fragmentation and rearrangement reactions that occur in photoexcited aniline cation. For the sake of simplicity, we generalize the possible outcomes of a solvated ion dissociation as follows:

$$A^+\cdot M_n \rightarrow A\{-a\}^+ + a\cdot M_n \quad (2)$$

$$A^+\cdot M_n \rightarrow A\{-a\} + a\cdot M_n^+ \quad (3)$$

$$A^+\cdot M_n \rightarrow A\{-a\}\cdot M_n^+ + a \quad (4)$$

$$A^+\cdot M_n \rightarrow A\{-a\}\cdot M_n + a^+ \quad (5)$$

where A{–a} is the major fragment resulting from loss of fragment a from parent A.

The results of this study have shown that, at high excitation energy, the familiar aniline fragment ions[36,37] appear for each of the solvents studied (e.g., Figures 3, 6, and 9). However, in no instance were the major fragment ions $A\{-a\}^+$ observed to be complexed with a solvent shell M_n. The lack of evidence for the reaction paths 4 and 5 may be taken to mean that (i) no dissociation occurs in solvated aniline, (ii) dissociation occurs only after solvent evaporation, or (iii) dissociation proceeds with the solvent attached to the undetected neutral fragment a. The last possibility is reasonable if the solvent M_n is hydrogen bonded to the amino group which is usually part of the departing neutral fragment a.

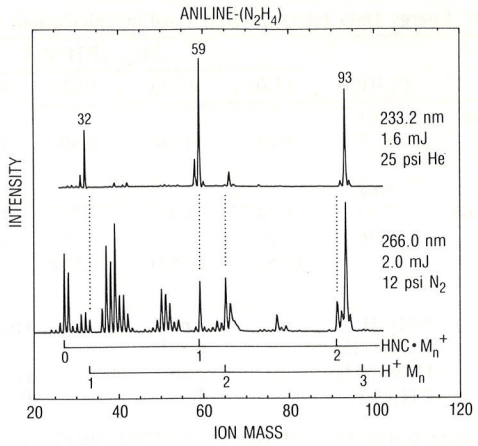

Figure 9. 1-C REMPI/MS of A–$(N_2H_4)_n$ clusters for different excitation conditions. The appearance of the fragment clusters HNC·$(N_2H_4)_n^+$ is evidence for a dissociation-induced charge-transfer mechanism. Numbers over peaks denote atomic mass units.

Reaction 3 can be explored by the present techniques only if either a or M_n has a lower ionization potential I_p than the major fragment A{–a}. In the case of aniline cation fragmentation, a does not usually satisfy this condition. However, if the solvent is suitably chosen, a charge transfer can occur from $A\{-a\}^+$ to a·M_n, thereby exposing the solvated dissociation mechanism. This set of circumstances is highlighted for the prominent low-energy A^+ dissociation that gives $C_5H_6^+ + HNC$ at an appearance potential of 11.3 eV.[56] For the solvated cation, the reaction can go by two paths depending on the I_p of the solvent M_n:

$$C_6H_5NH_2^+\cdot M_n \Rightarrow C_5H_6^+ + HNC\cdot M_n \quad (6)$$

$$\Rightarrow C_5H_6 + HNC\cdot M_n^+ \quad (7)$$

Reactions 6 and 7 are specific cases of the general reactions 2 and 3, respectively. The selectivity of reaction 7 to solvent I_p is dramatically demonstrated for N_2H_4 solvation. A dissociation-induced charge transfer is evident in Figure 9 by the presence of HNC·$(N_2H_4)_n^+$ for $n = 1, 2$. No analogous signals were observed for the solvents NH_3, CH_3OH, and H_2O (e.g., spectra that show fragmentation in Figures 12 and 13). This behavior is easily explained by comparing the I_p values of each constituent. A compilation of pertinent reference data[60-67] is given in Table I.

(52) Syage, J. A.; Wessel, J. E. *J. Chem. Phys.* **1988**, *89*, 5962. (b) Wessel, J. E.; Syage, J. A. *J. Chem. Phys.*, submitted.

(53) (a) Hollas, J. M.; Howson, M. R.; Ridley, T.; Halonen, L. *Chem. Hys. Lett.* **1983**, *98*, 611. (b) Tanaka, H.; Nishimoto, K. *J. Phys. Chem.* **1984**, *88*, 1052.

(54) Kosower, E. M; Huppert, D. *Ann. Rev. Phys. Chem.* **1986**, *37* 127, and references therein.

(55) Ireland, J. F.; Wyant, P. A. H. *Adv. Phys. Org. Chem.* **1976**, *12*, 131.

(56) Lifshitz, C.; Gotchiguian, P.; Roller, R. *Chem. Phys. Lett.* **1983**, *95*, 106.

(57) (a) Burgers, P. C.; Holmes, J. L.; Mommers, A. A.; Terlouw, J. K. *Chem. Phys. Lett.* **1983**, *102*, 1. (b) Burgers, P. C.; Holmes, J. L.; Mommers, A. A.; Terlouw, J. K. *Org. Mass Spectrom.* **1984**, *19*, 442.

(58) Strong evidence exists for the formation of HNC instead of HCN in the aniline fragmentation (ref 56 and 57). We assume that the I_p of HNC is comparable to or greater than HCN on the basis of the lower heat of formation for the latter molecule in its neutral and cationic state as compared to HNC. The I_p of HNC must certainly be greater than C_5H_6 to explain the charge residing on the latter fragment in the unsolvated reaction.

(59) (a) *Ionization Potential and Appearance Potential Measurements*; Levin, R. D., Lias, S. G., Eds.; 1971-1981 NSRDS-NBS 71; National Bureau of Standards: Washington, D.C.; 1982. (b) *Handbook of Chemistry and Physics*, 56th ed.; Weast, R. C., Ed.; CRC Press: Cleveland, OH, 1975.

(60) Lias, S. G.; Liebman, J. F.; Levin, R. D. *J. Phys. Chem. Ref. Data* **1984**, *13*, 695.

(61) Payzant, J. D.; Cunningham, A. J.; Kebarle, P. *Can. J. Chem.* **1973**, *51*, 3242.

(62) Lau, Y. K.; Ikuta, S.; Kebarle, P. *J. Am. Chem. Soc.* **1982**, *104*, 1462.

(63) (a) Lau, Y. K.; Kebarle, P. *Can. J. Chem.* **1981**, *59*, 151. (b) Meot-Ner, M. *J. Am. Chem. Soc.* **1984**, *106*, 1265.

(64) Ceyer, S. T.; Tiedemann, P. W.; Mahan, B. H.; Lee, Y. T. *J. Chem. Phys.* **1979**, *70*, 14.

(65) Frisch, M. J.; Pople, J. A.; Del Bene, J. E. *J. Am. Chem. Soc.* **1985**, *89*, 3664.

(66) McMillen, D. F.; Golden, D. M. *Ann. Rev. Phys. Chem.* **1982**, *33*, 493, and references therein.

(67) Arvis, M.; Devillers, C.; Gillois, M.; Curtat, M. *J. Phys. Chem.* **1974**, *78*, 1356.

In the neutral solvated molecule, anilne has a considerably lower I_p (7.7 eV) than any of the solvents and, hence, is the species to carry the positive charge upon ionization. Additional excitation causes the solvated cation to dissociate into fragments that have neutral I_p values greater than the aniline precursor (e.g., 8.97 eV for C_5H_6 and 13.6 eV for HNC[56-58]).[59] When aniline cation is uncomplexed or complexed with solvents whose I_p values are greater than either fragment, the most stable cation $C_5H_6^+$ is observed (reaction 6). However, when the solvent I_p is less than either fragment (but greater than aniline), as is the case for N_2H_4 (8.74 eV), then a charge transfer occurs (reaction 7).

Several other interesting features evident in Figure 9 merit discussion, namely, (i) charge transfer by reaction 7 occurs nearly exclusively at 233 nm, but only partially at longer wavelength (266 nm), and (ii) at 233 nm, unprotonated $N_2H_4^+$ monomer becomes a major product. The first observation is interesting because a much greater cluster ion energy is expected at the three-photon level for 233-nm (16.0 eV) versus 266-nm (14.0 eV) excitation. Yet the higher energy excitation seems to give more selective fragmentation. One explanation is that at lower energy, the rate of dissociation and charge transfer is slow compared to the absorption of a fourth photon, thus allowing higher threshold energy fragments to occur. At higher energy, the rate of dissociation and charge transfer at the three-photon level may predominate. Excess energy in $HNC{\cdot}(N_2H_4)_n^+$ is also consistent with the evaporation that apparently occurs, judging by the absence of signal for $n > 1$ for 233-nm excitation. This also explains the second observation. The substantial formation of $N_2H_4^+$ is intriguing in that the absorbing state of N_2H_4 monomer at about 233 nm is dissociative and therefore precludes MPI to form $N_2H_4^+$. The appearance of this ion signal in Figure 9 can be attributed to dissociation of the charge-transfer product $HNC{\cdot}N_2H_4^+$. This represents a situation where a dissociative molecule can be ionized by long-wavelength light by attaching a protecting group or sensitizer (in this case aniline) to carry the multiphoton excitation until dissociation-induced charge transfer can occur.

Intracluster Hydrogen and Proton Transfer

Two different reactions representing hydrogen or proton transfer were examined, depending on whether the aniline cation A^+ or the solvent shell M_n acts as the donor (acid) or acceptor (base). These pathways, which require a cluster ion dissociation, are represented by

$$A^+{\cdot}M_n \Rightarrow AH^+{\cdot}M_{n-1} + M\{-H\} \quad \text{H transfer} \quad (8)$$

$$\Rightarrow A\{-H\} + H^+M_n \quad H^+ \text{ transfer} \quad (9)$$

where M{–H} and A{–H} are the radicals representing loss of an H and H^+ from M and A^+, respectively. Since the cluster ion charge density is localized on aniline, it is correct to consider reaction 8 as a hydrogen abstraction. Reactions 8 and 9 become equivalent when A = M, which corresponds to the reaction involving neat solvent cluster ions.

Dissociative Hydrogen Transfer. The gas-phase bimolecular counterpart to reaction 8 is given by

$$A^+ + M \Rightarrow AH^+ + M\{-H\} \quad (10)$$

This reaction may be expressed by a thermodynamic cycle such as

$$\begin{aligned} A^+ + e^- &\Rightarrow A & -I_p(A) \\ M &\Rightarrow M\{-H\} + H & D_H(M\{-H\}) \\ H &\Rightarrow H^+ + e^- & I_p(H) \\ A + H^+ &\Rightarrow AH^+ & -D_{H^+}(A) \end{aligned} \quad (11)$$

This leads to the useful expression for the gas-phase reaction enthalpy

$$\Delta H_g = I_p(H) - I_p(A) + D_H(M\{-H\}) - D_{H^+}(A) \quad (12)$$

The I_p values are ionization potentials, and the D values are bond energies which are written to be interpreted as a hydrogen affinity (D_H) and a proton affinity (D_{H^+}).

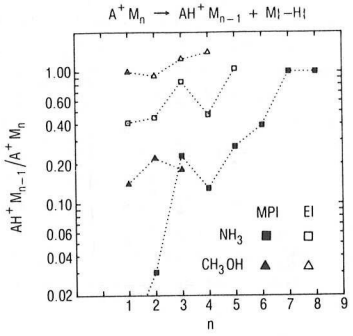

Figure 10. Observed ratio of protonated to unprotonated solvated aniline cation as a function of solvent shell size n. Results of the intracluster proton-transfer reaction are shown for NH_3 and CH_3OH solvation and MPI and EI excitation. The data represent the average of several spectra at 0.1–0.2 mJ/pulse at 295 nm.

The expression for the gas-phase enthalpy may be modeled to include the energetics of stepwise solvation. An expression for the solvated enthalpy ΔH_s as a function of solvent size n (see Appendix) is given by

$$\Delta H_{s,n} = \Delta H_g + \sum_{i=1}^{n} \Delta E_{i,i-1}(A^+M_i) - \sum_{i=2}^{n} \Delta E_{i-2,i-1}(AH^+M_{i-1}) \quad (13)$$

The ΔE terms are solvation bond energies for successive addition of M to A^+ and AH^+, respectively. In the case of reaction 8, the summation terms account for solvent stabilization of the reactant and products, respectively. In the interest of adopting a physical picture, it is somewhat correct to view the contribution of $\Delta E(A^+M_i)$ as a reduction in $I_p(A)$ and $\Delta E(AH^+M_i)$ as an increase in $D_{H^+}(A)$ resulting from solvation.

For the value of $n = 1$, the second summation term does not contribute to $\Delta H_{s,n}$. This is physically realistic since a comparison of reactions 8 and 10 shows that only the reactant can experience a stabilization for the minimum level of solvation $n = 1$. This situation has the curious effect of *increasing* the enthalpy of the reaction compared to the gas-phase bimolecular value. The effect of further solvation on $\Delta H_{s,n}$ depends on the relative values of $\Delta E(A^+M_i)$ and $\Delta E(AH^+M_i)$ as a function of n. Usually, though, the latter term dominates, in which case $\Delta H_{s,n}$ decreases by further increasing n. This predicts a turnover region at $n = 1$, which we discuss shortly.

At this point we examine the extent of aniline protonation by hydrogen transfer (reaction 8) as a function of solvent (M and n) and excitation (MPI and EI). Only the results for NH_3 (Figures 3 and 4) and CH_3OH (Figures 6 and 7) were judged to be of sufficient quality and completeness to be useful. We present the results describing reaction 8 in a more suitable form in Figure 10. The following pertinent observations can be made: (i) the formation of protonated cluster ions $AH^+{\cdot}M_{n-1}$ was greater for solvation by CH_3OH than for NH_3, the latter solvent exhibiting a rather abrupt threshold at $n = 3$ by MPI; (ii) the $AH^+{\cdot}M_{n-1}$ ions were found in much lower yield relative to the precursor $A{\cdot}M_n^+$ by MPI versus EI; (iii) the stability of the $A^+(NH_3)_4$ cluster ion discussed earlier is also evident by the dip at $n = 4$ in Figure 10, indicating resistance toward dissociative hydrogen transfer; (iv) in contrast to microsolvated aniline ions, ionization of neat microsolvent clusters resulted in nearly exclusive formation of protonated cluster ions (Figures 4 and 7 and previous studies[13,44,68-70]).

The results presented here demonstrate that the incremental addition of solvent molecules can have profound effects on a

(68) Echt, D.; Kreisle, D.; Knapp, M.; Recknagel, E. *Chem. Phys. Lett.* **1984**, *108*, 401.
(69) (a) Kay, B. D.; Castleman, A. W. *J. Phys. Chem.* **1985**, *89*, 4867. (b) Mori, Y.; Kitagawa, T. *Chem. Phys. Lett.* **1986**, *128*, 383, 389.
(70) (a) Shinohara, H.; Nishi, N.; Washida, N. *J. Chem. Phys.* **1986**, *84*, 5561. (b) Choo, K. Y.; Shinohara, H.; Nishi, N. *Chem. Phys. Lett.* **1983**, *95*, 102.

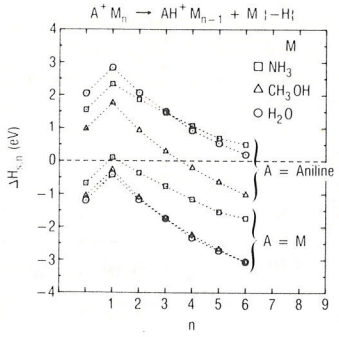

Figure 11. Calculated stepwise solvation enthalpies for intracluster proton transfer to give protonated aniline (A = aniline) in seeded clusters and protonated solvent (A = M) in neat solvent clusters. The left-hand most data are for the gas-phase reactions. $\Delta E(A^+M_i)$ values for $i \geq 2$ could not be found for CH_3OH and H_2O; therefore, values for NH_3 were used (cf. Table I). Actual values should be larger, meaning that the $\Delta H_{s,n}$ curves for CH_3OH and H_2O should fall off less rapidly than shown.

reactive molecule. An attempt to model this behavior using expressions such as eq 12 is hampered by the lack of an extensive base of data for the energetics of solvation. We have therefore made an effort to compile in Table I a set of available data that best represents the properties of the microsolvated clusters considered here. For lack of available data on mixed clusters, we have assumed that the presence of aniline in the solvent clusters does not appreciably change the stepwise solvation energies measured for neat clusters. At the very least, it is plausible to assume that the correction should be nearly uniform for all the solvents. Data on the solvation energies of unprotonated cations are very limited; hence, we used the values for NH_3 for the other solvents.[71] The qualitative differences in $\Delta H_{s,n}$ for each solvent are therefore due to the other terms in eq 12 and 13. The gas-phase terms that appear in eq 12 fortunately are well-known[72] and listed in Table I.

The calculated enthalpies $\Delta H_{s,n}$ for protonation of stepwise solvated cluster ions by reaction 8 are presented in Figure 11 for the case of aniline nucleation (A = aniline) and neat solvent clusters (A = M). Due to the limitations discussed in the previous paragraph, the uncertainty in the absolute energies is probably no better than 0.5 eV; however, the relative energies for different solvents and solvent sizes are judged to be valid to about 0.2 eV. Despite these caveats, the calculated results immediately bear out a number of experimental observations. First, the enthalpy of protonation is about 2 eV more exothermic for the neat versus aniline-seeded cluster ions. The basis for this result is the lower I_p of aniline compared to the solvent molecules. This accounts for a lower heat of formation on the reactant side of reaction 8 and therefore a higher enthalpy for reaction. Second, the enthalpy of protonation to form $AH^+\cdot M_n$ is more exothermic for CH_3OH than for NH_3. This explains the higher observed yield of protonated product for the CH_3OH solvent in Figure 10. Third, the calculation predicts an increase in enthalpy for complexation with a single solvent molecule (i.e., $n = 1$), as noted before. However, upon additional solvation, the proton-transfer reaction is stabilized and becomes more favorable than in the gas phase. This occurs because the energy of solvation for protonated ions is greater than for unprotonated ions (Table I).

The turnover region in Figure 11 is physically realistic and not without precedent experimentally. For example, the gas-phase reaction

$$NH_3^+ + NH_3 \rightleftharpoons NH_4^+ + NH_2 \qquad (14)$$

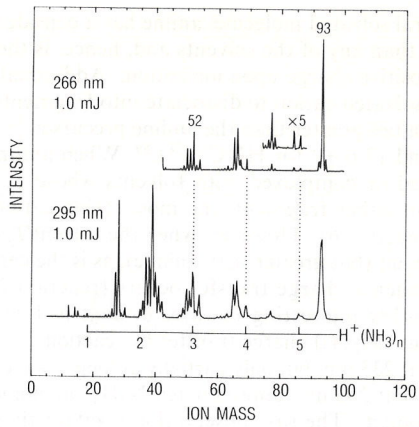

Figure 12. Low-mass region of the 1-C REMPI/MS of $A-(NH_3)_n$ clusters showing evidence for a critical solvent size of $n = 3$ for dissociative proton transfer to form $H^+(NH_3)_n$. Numbers over peaks denote atomic mass units.

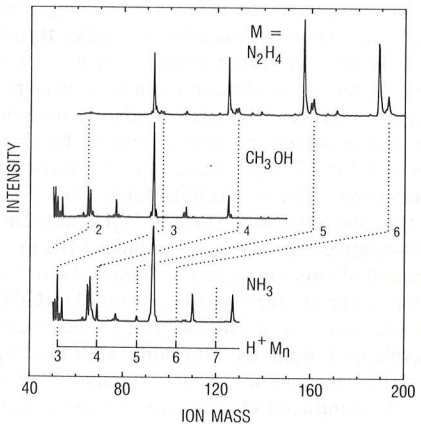

Figure 13. 1-C REMPI/MS of A^+M_n clusters showing evidence for a critical solvent size in various solvents for dissociative proton transfer to form H^+M_n. Pulse energies were about 1.0 mJ (295 nm) for M = NH_3 and CH_3OH and 0.40 mJ (233 nm) for N_2H_4.

is about 1.1 eV exothermic[73] and reacts with near unit collision efficiency at ambient temperatures.[73,74] The cluster reaction

$$NH_3^+\cdot(NH_3)_n \rightleftharpoons NH_4^+\cdot(NH_3)_{n-1} + NH_2 \qquad (15)$$

on the other hand, has an equilibrium constant of $K_{eq} < 1$ for $n = 1$ and $K_{eq} \gg 1$ for $n > 1$ (Figure 4 and elsewhere[13,44]). Very similar behavior has been reported for the slightly more exothermic reaction involving H_2O cluster protonation.[70] In fact, these experimental observations are surprisingly well described by the model in Figure 11, where reactions 14 and 15 are calculated to be exothermic for all cases *except* when $n = 1$. Other examples in which gas-phase ion molecule reactions are quenched in small cluster ions have been reported by Garvey and Bernstein.[12] They also attribute this to stabilization of the reactant side by the energy of complexation.

Dissociative Proton Transfer. A thermodynamic cycle appropriate to reaction 9 can be written that gives the gas-phase reaction enthalpy:

$$\Delta H_g = I_p(H) - I_p(A) + D_H(A\{-H\}) - D_{H^+}(M) \qquad (16)$$

where the terms have been defined before. The addition of terms to include the energetics of stepwise solvation is similar to that described in the Appendix and is given by

$$\Delta H_{s,n} = \Delta H_g + \sum_{i=1}^{n} \Delta E_{i,i-1}(A^+M_i) - \sum_{i=2}^{n} \Delta E_{i,i-1}(H^+M_i) \qquad (17)$$

(71) Cation solvation energies are also available from measurements of solvent induced shifts of I_p. Wallace and co-workers (ref 21) have measured the 2-C REMPI ionization threshold of 2-aminopyridine complexed to NH_3, CH_3OH, and H_2O, obtaining very similar values (cf. Table I). The addition of a second solvent molecule, however, gave very dissimilar results. This has been attributed to large geometry changes upon ionization, in which case, the measured thresholds represent vertical and not adiabatic values of I_p.

(72) Moylan, C. R.; Brauman, J. I. *Ann. Rev. Phys. Chem.* **1983**, *34*, 187.

(73) Conaway, W. E.; Ebata, T.; Zare, R. N. *J. Chem. Phys.* **1987**, *87*, 3453.

(74) Adams, N. G.; Smith, D.; Paulson, J. F. *J. Chem. Phys.* **1980**, *72*, 288.

(75) Shinohara, H.; Sato, K.; Achiba, Y.; Nishi, N.; Kimura, K. *Chem. Phys. Lett.* **1986**, *130*, 231.

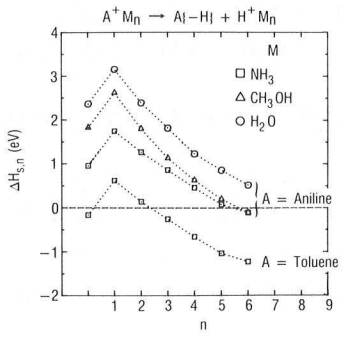

Figure 14. Calculated stepwise solvation enthalpies as a function of solvent and shell size n for dissociative proton transfer. Calculated results are compared for A = aniline and toluene. See the caption for Figure 11 for additional explanation.

Here, the ΔE terms are solvation energies for successive addition of M to A^+ or H^+, respectively.

The appearance of the product H^+M_n in the REMPI mass spectra for M = NH_3 is shown in Figure 12 for two different excitation wavelengths. The results for NH_3 are compared to related spectra involving the microsolvents N_2H_4 and CH_3OH in Figure 13. From these and other spectra, the following observations are reached: (i) H^+M_n formed from $A^+{\cdot}M_n$ precursor was observed for NH_3 and N_2H_4 with a solvent size threshold of $n \geq 3$; (ii) no protonated solvent H^+M_n was observed for CH_3OH or H_2O up to values of $n = 5$, representing the limit to acceptable signal-to-noise for these solvents. The possibility exists for H^+M_n to be formed by nonresonant MPI of neat solvent clusters M_{n+1} (i.e., reaction 8 or 9 where A = M). The observation of a solvent size threshold for H^+M_n formation, however, argues against this being the case; ionization of neat solvent clusters would favor low values of n resembling the neutral cluster size distribution. Assessing the intensity of some signals is also difficult when they are coincident with other masses. For instance, the signal for $H^+(NH_3)_3$ at 52 amu is judged to be real and significant by comparison of the 52-amu aniline fragment signal strength in the absence of NH_3. Similarly $H^+(CH_3OH)_2$ is not considered to contribute to the aniline fragment signal at 65 amu in Figure 13; a view supported by the absence of signal for larger values of n.

Brutschy et al.[34] recently reported evidence for dissociative proton transfer involving toluene and p-xylene solvated with NH_3, CH_3OH, and H_2O. These investigators, likewise, observed a threshold size effect. The relative ordering of the n threshold values for the various solvents was consistent with that observed in the present work, although the absolute values in the former work were shifted to smaller n. These results are in accord with the model for stepwise solvations developed above. The solvated enthalpies $\Delta H_{s,n}$ for reaction 9 were calculated by using eq 16 and 17, along with the solvation energies $\Delta E_{i,i-1}$, the gas-phase I_p values, and bond energies listed in Table I. The results are plotted in Figure 14. A notable feature again is the predicted increase in enthalpy at the first level of solvation $n = 1$ due to stabilization of the reactant side of reaction 9 without an offsetting stabilization of the products. Subsequent solvation, however, stabilizes the products to a greater extent than the reactants so that the overall influence of solvation is to increase K_{eq} relative to the gas phase. A second feature is that the ordering of exothermicities, $NH_3 > CH_3OH > H_2O$, is in agreement with the present results and those of Brutschy et al.[34] This trend is most strongly correlated with the proton affinity $D_{H^+}(M)$ (eq 16 and Table I). A third feature is that the calculated solvation enthalpies $\Delta H_{s,n}$ are more exothermic for A = toluene, thus explaining the smaller threshold values of n reported by Brutschy et al. for that system. The calculated curve for the reaction involving toluene–$(NH_3)_n$ is plotted in Figure 14, although the calculated curves for all solvents are shifted in energy from the aniline–$(NH_3)_n$ data by essentially a constant representing the differences in the I_p and hydrogen-bond dissociation energy $D_H(A\{-H\})$ of the aromatic cations. Because the latter quantity is coincidentally the same for both aniline and toluene (Table I), the overriding property that most accounts for the differences in reaction energies is the I_p (eq 16).

To conclude the discussion, we issue a few caveats regarding the analyses presented thus far. Although the qualitative behavior of stepwise solvation in this and other work is well predicted, the model does not precisely describe the experimental conditions that give rise to the specific threshold values of n. This is due to the nature of the experiment, which permits not equilibrium studies but rather extent of reaction. The observed yield of products is that which occurs during the residence time of the parent ions in the excitation volume of the TOF mass spectrometer. This time (which ranges from ~1 to 4 μs) increases with mass, thus favoring slightly the detection of products from larger cluster ions. For these reasons, the discussion has centered on a comparison of solvation enthalpies $\Delta H_{s,n}$ rather than free energies $\Delta G_{s,n}$. This decision was also made because the cluster temperatures and reaction entropies are not well defined. However, the entropies are certainly positive for the reactions discussed; hence, the calculated free energies $\Delta G_{s,n}$ are smaller than $\Delta H_{s,n}$, which would give a stronger correlation (in terms of threshold values of n) with the observed results.

Summary and Conclusions

Studies that afford a view of stepwise solvation on a molecular level are basic to bridging our understanding of gas-phase and condensed-phase chemistry. We have reported on unimolecular dissociation and bimolecular intracluster hydrogen-transfer and proton-transfer reactions involving aniline cation bonded to specific solvent shell sizes consisting of either NH_3, N_2H_4, CH_3OH, and H_2O. Although, considerable work has been reported in the past on proton-transfer properties in small molecules, much less information is known about the stepwise solvation of large reactive molecules, especially regarding unimolecular dissociation. The major results of this work are summarized below.

The prominent aniline cation gas-phase dissociation

$$C_6H_5NH_2^+ \rightarrow C_5H_6^+ + HNC$$

was investigated as a function of solvent and solvent size. For all solvents studied except N_2H_4, only uncomplexed $C_5H_6^+$ and higher threshold energy fragment ions were observed. For N_2H_4 solvation, however, a major reaction pathway forming $HCN{\cdot}(N_2H_4)_n^+$ became apparent. This reaction is due to a dissociation-induced charge transfer that occurs because the I_p of N_2H_4 lies above that of aniline but below that of the fragment species.

Intracluster hydrogen and proton transfer in microsolvated aniline cation was less favored for any donor/acceptor combination that in neat solvent cluster ions. The protonation of aniline by the dissociative hydrogen transfer from solvent

$$A^+{\cdot}M_n \rightarrow AH^+{\cdot}M_{n-1} + M\{-H\}$$

was greater when solvated by CH_3OH than by NH_3. For REMPI excitation, the latter reaction required a critical solvent size of $n > 3$. For 20- and 60-eV EI excitation, AH^+ was formed in greater abundance relative to REMPI excitation and without any apparent threshold value for n. The analogous reaction of dissociative proton transfer from aniline cation to solvent

$$A^+{\cdot}M_n \rightarrow A\{-H\} + H^+{\cdot}M_n$$

also exhibited a critical solvent size effect for REMPI excitation, depending on the isolated solvent molecule proton affinity and the incremental change in this value due to complexation. Consequently, thresholds for formation of H^+M_n were observed for NH_3 ($n \geq 3$), N_2H_4 ($n \geq 2$), CH_3OH (not seen, $n > 4$), and H_2O (not seen, $n > 4$).

The solvation dynamics for aniline cation reactivity showed excellent correlation with a model developed to take account of the change in the gas-phase ion–molecule reaction enthalpy resulting from successive addition of a solvent molecule. The model also predicts a turnover region for ion molecule protonation reactions such that the gas phase enthalpy actually increases for the minimal level of solvation (i.e., $n = 1$) before decreasing for subsequent solvation. The physical basis for this effect is explained.

The work presented here is illustrative of the profound effect that a small number of solvent molecules can have on the course of a chemical reaction. Considerable experimental and theoretical refinements can be expected in the near future to supplant the qualitative dependences reported here. Experimentally, the techniques are at hand to probe state-selective and time-resolved properties of size-specific clusters. We may therefore look forward to more fundamental insights into solvated reaction mechanisms on a molecular level.

Acknowledgment. I am grateful for the assistance of R. A. Hertz and M. L. Homer in the operation of the hydrazine source. This work was funded by the Aerospace Sponsored Research Program.

Appendix

The expressions for the solvent size-specific reaction enthalpies that appear in eq 13 and 17 are formulated by adding additional terms to the gas-phase thermodynamic cycles to account for stepwise solvation. As an example, reaction 8

$$A^+{\cdot}M_n \Rightarrow AH^+{\cdot}M_{n-1} + M\{-H\}$$

can be broken down to the form

$$\begin{aligned}
A^+M_n &\Rightarrow A^+M_{n-1} + M & \Delta E_{n,n-1}(A^+M_n)\\
A^+M_{n-1} &\Rightarrow A^+M_{n-2} + M & \Delta E_{n-1,n-2}(A^+M_{n-1})\\
&\vdots \quad \vdots & \vdots\\
A^+M &\Rightarrow A^+ + M & \Delta E_{1,0}(A^+M_1)
\end{aligned}$$

$$\begin{aligned}
A^+ + e^- &\Rightarrow A & -I_p(A)\\
M &\Rightarrow M\{-H\} + H & D_H(M\{-H\})\\
H &\Rightarrow H^+ + e^- & I_p(H)\\
A + H^+ &\Rightarrow AH^+ & -D_{H^+}(A)
\end{aligned}$$

$$\begin{aligned}
AH^+ + M &\Rightarrow AH^+M_1 & -\Delta E_{1,0}(AH^+M_1)\\
AH^+M + M &\Rightarrow AH^+M_2 & -\Delta E_{2,1}(AH^+M_2)\\
&\vdots \quad \vdots & \vdots\\
AH^+M_{n-2} + M &\Rightarrow AH^+M_{n-1} & -\Delta E_{n-1,n-2}(AH^+M_{n-1})
\end{aligned}$$

It is straightforward to show that by summing the solvation terms, one obtains eq 13. The expression given by eq 17 for reaction 9 follows in a similar manner.

Registry No. NH_3, 7664-41-7; N_2H_4, 302-01-2; CH_3OH, 67-56-1; H_2O, 7732-18-5; $C_6H_5NH_2^+$, 34475-46-2.